European Journal of Molecular & Clinical Medicine
ISSN 2515-8260 Volume 07, Issue 06, 2020

Finite Element Analysis Of Porous Aluminium Aa3003 Alloy Under Compression And Bending Loading

Basem Mohysen Al-Zubaidy[1], AbdulRaheem Kadhim AbidAli[2], Noor Hmoud Athaib[3]

[1,2,3]*Department of Metallurgical Engineering, College of Materials Engineering, University of Babylon, Babylon, Iraq*

Email: [1]mat.basem.mahsn@uobabylon.edu.iq; [2]aaabidalieng@gmail.com; [3]noorhmoud9@gmail.com

Abstract: Recently, the demand to analyse the performance of metal foams is increased due to the increase in use of them in different engineering applications. In this study, two types of porous metals were finite element (FE) modelled in terms of pore size and distribution (uniform and random) with three pores' volume fractions (15, 40, and 65%). Uniformly distributed pores were analysed based on a tetrahedron cell. Conversely, the data of the size and location of each pore in the random porous metal were generated using Microsoft excel software. Two types of test samples were modelled, compressive and bending. The results showed that the location of the maximum Von-Mises stress for uniformly pores metal in the compression test was located in the vertical walls between pores. Whereas it located in the upper or the lower surface at the centre of the bending sample. The samples with random distribution pores show more complex behaviour due to the non-uniform thickness of walls between the pores. However, the maximum stress found to be located at the thinner vertical walls between the pores for the compression sample. Nevertheless, the maximum stress was located at the thinnest horizontal walls, near the location of the maximum bending moment.

Keywords: Finite element analysis, metal foams, porous metals, random porosity, uniform porosity.

1. INTRODUCTION

Porous materials are a class of functional-structural materials with better physical and mechanical properties [1]. Metal foams are metal components with solid parts (for example aluminium) and gas-parts (pores) having a big space in the element. These materials can be classified in many terms such as the pores types - open or close pores [2] or may be classified based on the percentage of pores into low, medium and high porosity. Moreover, porous metals can be natural and artificial based on the manufacture processes [3-5].

Porous materials can offer excellent unique properties. These materials have a massive scientific and technological interest due to their extremely high surface-to-volume ratio. Atoms, ions and molecules can interact with the porous materials not only on the outer surface but also inside the pores. Therefore, porous materials have been traditionally used in gas adsorption (separation), catalysis, ion exchange, and many of these applications have achieved commercialized production [6]. Porous materials are extremely lightweight compared to their equivalent solid section. Metal foams often weighing approximately 5% - 25% to the solid metal. The advantage of being porous allowing gas and liquid to pass through their cellular

structure as a filter, low thermal conductivity, high compressive strength, very good sound absorption capacity, biomaterial and flame-retardant property and non-flammability [2].

The study of the mechanical properties of metallic foams remains an important topic. The most foam applications are primarily load-bearing (e.g., for the sandwich structures). However, the main properties of foams are functional (e.g., acoustic, thermal or surface area) which required minimal mechanical properties to prevent damage or failure [7]. Mechanical properties depend on the density of the body and on the internal structure, the structure used, the size of the pores used, their distribution, and types of porous material (closed or open) [3].

All mechanical and physical properties depend basically on the relative density ρ/ρ_s (or porosity) non-linearly with the coefficient a and the structural constant k, as in the relation below [8]:

$$\frac{p}{p_s} = k\left(\frac{\rho}{\rho_s}\right)^a \quad (1).$$

A considerable amount of literature has been published on porous metals. Most of these studies focused on the experimental investigation of the mechanical properties of these materials, however, more recent attention has focused on the using of the finite element methods to predict the behaviour of such materials under different conditions. For instance, Nammi, et al [9] used the finite element to evaluate the stiffness and mechanical response of closed-cell aluminium foam which represented using repeating unit-cell constructed from the tetrakaidecahedron structure. The results showed that the plateau phase stress-strain characteristics of this model are more representative of real aluminium foam. On the other hand, Kader, et al [10] used the numerical simulation of a plate-impact experiment to elucidate the shock propagation through closed-cell aluminium foam and its effect on cell-wall deformation and pore collapse. The full 3D foam geometry was adopted to develop using the X-ray computed microtomography approach followed by using the finite element method understanding detailed macrostructural response due to shock propagation. Good correlations were observed between experimental data and finite element (FE) predictions. Similarly, a both of the experiments and finite element modelling were used by Soro, et al [11] to study the effect of various porosity levels on the mechanical properties of commercially porous pure titanium. The results of modelling showed that the pore shape and the porosity level have a significant effect on the behaviour of porous metal. Recently Tamai, et al. [12] investigated the behaviour of porous AA6061 alloy with aligned unidirectional pores. They studied the distributions of the equivalent plastic strain under compressive loading using digital image correlation and finite element analyses. They found that the material undergone three deformation modes after the plastic collapse of the cell walls started with plastic buckling followed by fracture, and finally rapid densification. In the same way, Nishi et, al [13] analysed the mechanical properties of a cubic unidirectional porous copper sample subjected to high-velocity impact. They used a high-speed video camera and the computational simulations to compare the results of the deformed shape in both experimentally prepared sample and simulated one. In both cases, the compression results in a high pressure near the pore. Likewise, Tomažinčič et, al [14] used experimental and Numerical simulations to compare three types of planar cellular structures auxetic, auxetic-chiral and hexagonal in terms of static and low-cycle durability. The three samples were made from an aluminium alloy AA7075-T651 and tested at different loading amplitudes. The observation showed good agreement between the simulated and experimental results. Overall, these studies highlight the need for more understanding of the behaviour of both types of porous metals (uniform and random).

In this study, foams of aluminium alloy AA3003 and porous aluminium alloy AA3003 were analysed to predict the mechanical behaviour (compression and bending) using finite element

analysis taking into consideration generation of three-dimensional samples with uniform and random distribution of pores in the metal matrix, in addition to the study of the effect of the pore size, porosity and pores distribution on the mechanical behaviour of the metal foams and porous metals.

Material Data

The materials used in this study were the AA3003 aluminium alloys, the nominal composition of which is shown in Table (1).

Table 1. Nominal chemical compositions of the alloys used in this study.

Component	**Si**	**Cu**	**Fe**	**Mn**	**Zn**	**Al**
Percentage%	0.6	0.05-0.20	0.70	1.0-1.5	0.1	96.8-99

To measure the mechanical properties of the AA3003 alloy, several standard tensile test samples of this alloy were tested using a universal testing machine with a crosshead travel speed of 1.0, mm/min. The data were collected at 50 Hz. These data were then transformed into true stress - true strain using Equations (2) and (3) [15] to be suitable for use in the FE modelling.

$$\epsilon_{true}$$

$$\sigma_{true} = \sigma_{eng.}(1 + \epsilon_{eng.}) \quad (3)$$

where: ϵ_{true}: True strain

$\epsilon_{eng.}$: Engineering strain

σ_{true}: True stress

$\sigma_{eng.}$: Engineering stress

The curve was then separated into elastic and plastic regions. From the elastic region, the only data required was the elastic modulus. On the other hand, for the plastic deformation region smooth-curves of this region were fitted. The fitting process reduced the number of data points from several thousand to only 15 points to reduce the time required to process the model, as seen in Table 2.

Table 2. True stress- true strain data used for modeling

Plastic strain	**Plastic stress (Pa)**
0	29000000
0.00611	41205660
0.01222	48669000
0.01834	55213620
0.02445	59506440
0.03056	63325160
0.03667	67669770
0.04278	71540270
0.0489	74936670
0.05501	77858970
0.06112	80307150
0.06723	82281230
0.07335	83781210
0.07946	84807080
0.08557	85358840

Computational Models: Foam Geometry

In this work, two types of porous metal (metal foam) (i.e. the uniform and random porous metal) were modelled to subject to compressive and bending tests. The compressive test specimens were cubes with (25x25x25 mm) taken from [16] On the other hand, the dimensions of the specimens used for the bending test were (240x50x10). Each type of porous metals has different modelling procedure with different volume fraction (porosity) (15 %, 40 %, 65%). In general, the pores were assumed to have a spherical shape.

Uniform Porous Metal (Metal Foam)

This type has uniform pores in terms of the volume (diameter) and their distribution. The data used for geometry design (shown in Table (3)) depended on the volume fraction, the number of pores and the radius of each pore. The number of pores was assumed to be (125) and (480) pores for the compression and bending specimen respectively. Each sample was divided into small cells depending on the number of pores. All cells were made of cubes with a central spherical cavity.

Table 3. Geometrical data of the uniform distribution porous metal (metal foam) used in FE study for the compressive and bending test.

Specimen type	Dimensions (mm)	Cube dimensions (mm)	Porosity	Pore diameter (mm)	Number of pores	Type of foam cell
compressive	25x25x25	5x5x5	15%	3.3	125	Close
			40%	4.6		Close
			65%	5.4		Open
bending	240x50x10	5x5x5	15%	3.3	480	Close
			40%	4.6		Close
			65%	5.4		Open

Random Porous Metal (Metal Foam)

In the design of the geometry used for compressive and bending specimens with random pores, the data used (i.e. pores sizes and distribution) were generated using the Microsoft Excel software. Certain functions in this software were used to generate lists of pores radii and locations (x,y,z coordinates) in 3D specimens. The pores diameters were ranged from (3 to 6) mm depending on the random function. Some data of the random distribution pores (radii and locations) are shown in Table (4).

Table (4): Some of the random pore data for radius and location of a random distribution porous metal in FE study.

Pores Dimensions		Location		
Radius	**Volume**			
mm	**mm^3**	**x**	**y**	**z**
0.2489064	0.0645619	8	7	8
0.0410732	0.0002901	2	2	3
0.8876368	2.9280212	3	7	2
0.068346	0.0013366	1	1	2

0.9933628	4.1038552	5	4	5
0.4786381	0.4590819	5	9	7
0.214941	0.0415744	6	4	9
0.9550236	3.646789	7	1	2
0.756671	1.813801	5	4	8

Boundary Conditions and Meshing

The boundary conditions were the same for each compressive test sample (uniform and random distribution pores). All the degrees of freedom on the lower face of the sample were fixed, whereas the upper face of the cube had one free degree of freedom (Y translation) and that face was loaded by applying a displacement of (2.5mm). This value is equal to 10 % of the total height of the sample. On the other hand, the boundary conditions for the three-point bending test were applied by fixing two lines of the samples' lower surface and applying a displacement of (1mm) on the centre line of the upper face as shown in Fig. 1.

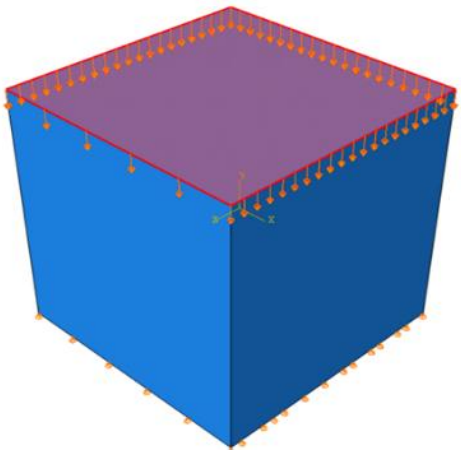

(a) compression specimen

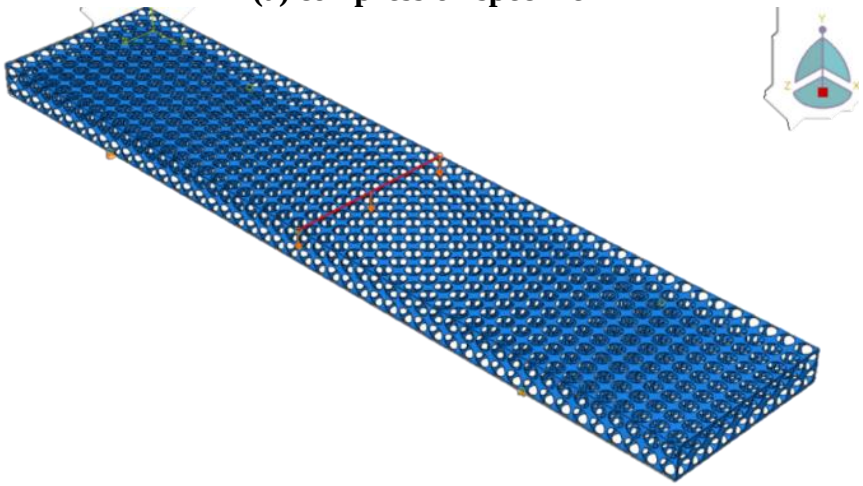

(b) three-point bending specimen.

Fig. 1. Boundary condition for the two types of spacemen

A tetrahedron type element (ten-node C3D10M elements) was used for the meshing in all cases of the bending and compression as shown in Figs. 2 and 3.

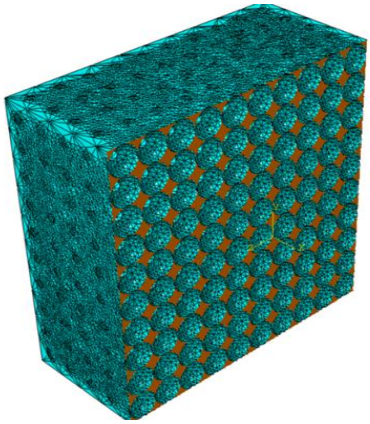

(a) uniform pore distribution (vertical section)

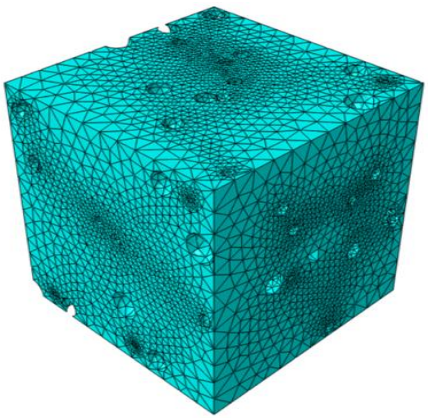

(b) random pore distribution.

Fig. 2. Tetrahedron mesh of compressive specimen

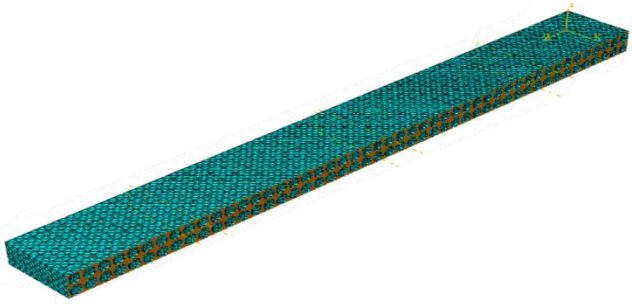

(a) uniform pore distribution (vertical section).

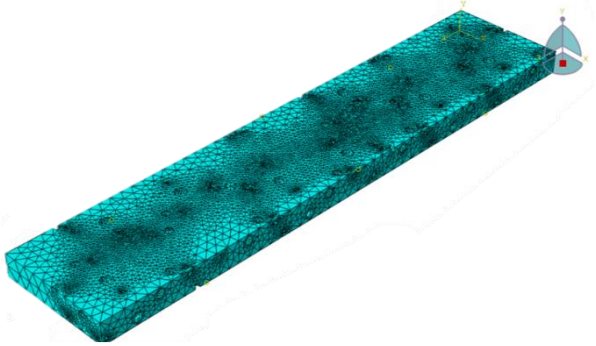

(b) random pore distribution.

Fig. 3. Tetrahedron mesh of bending specimen.

2. RESULTS AND DISCUSSION

Compression Test Samples

Fig. 4 shows the von misses stress contour for compression sample with uniform pore distribution (65 % porosity). As can be seen, the maximum stresses located in the vertical walls between pores whereas the minimum value of stresses lies in the horizontal region between the pores. It is clear that the compression tends to deform the pore from the spherical to elliptical shape with a preferred longer axis perpendicular to the load direction. On the other hand, for the sample with the same porosity (65%) with random pores size and distribution (Fig. 5), the regions of maximum and minimum stresses are difficult to be predicted. However, it found to be through the thinner area between the pores for the maximum stress, whereas the minimum stress can be seen in the thickest horizontal wall between the pores. Moreover, the deformation

of the pores shows very high non-uniformity compared to that for pores uniform samples due to the non-evenly distribution of pores in addition to the differences in pore size.

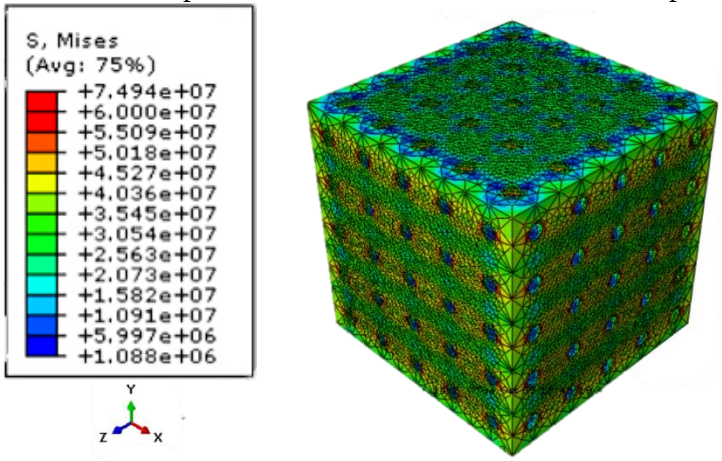

(a) 3D sample.

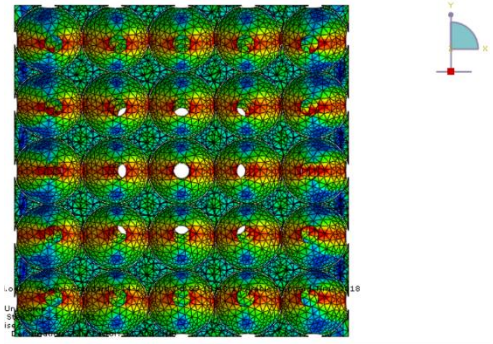

(b) vertical cross-section of the same sample in (a).

Fig. 4. Von-mises equivalent stress distribution of a 65 % volume fraction sample with uniform distribution of pores under compressive loading

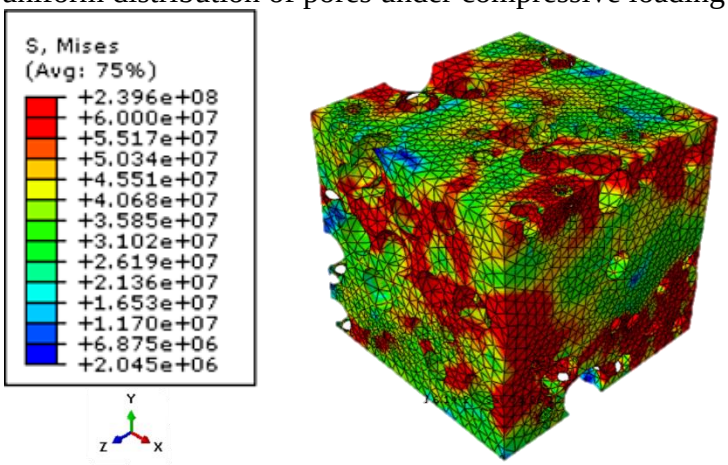

(a) 3D sample.

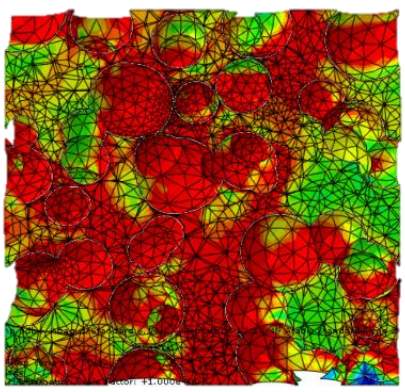

(b) vertical cross-section of the same sample in (a).

Fig. 5. Von-mises equivalent stress distribution of a 65 % volume fraction sample with a random distribution of pores under compressive loading

The effect of porosity (the volume fractions of pores) on the maximum Von-Mises stress for uniform and random distribution in compression specimens is shown in Fig. (6). The maximum Von-Mises stress for uniform pores shows a slight increase with increasing the porosity from 15 to 40 % due to the decrease in the thickness of the vertical walls of the pores which carry the load. However, the maximum stress decreased by increasing the porosity to 65% due to the change of the porosity type from the close to open pore which increases the effect of buckling of these walls, which develops stresses in more directions and other than the direction of the maximum stress. On the other hand, the sample with random distribution pores shows higher stresses because it contains some regions with much thinner walls than the walls of uniform distribution sample. These stresses increase with increasing the porosity despite the effect of buckling.

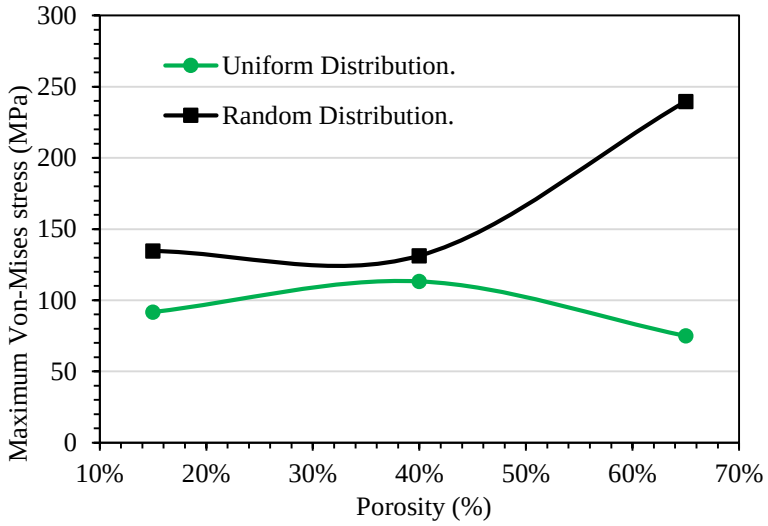

Fig. 6. The effect of pores volume fraction (porosity) on the Von-mises equivalent stress distribution of compression specimens for both uniform and randomly distributed pores.

Bending Test Samples

In the samples with uniform distribution of the pores and subjected to bending loading the maximum stress can be noticed in the top and bottom regions of the specimen near the loading area due to the similarity of pore size and the symmetry of pores distribution. The distribution of the stresses is almost uniform, where the maximum stress located at the upper surface (the compression region) or at the bottom surface (the tension region) under the loading line. The

stresses gradually decrease until they reach the lowest value at the ends of the sample as shown in Fig. (7). This behaviour is very similar to that shown by the samples without any pores.

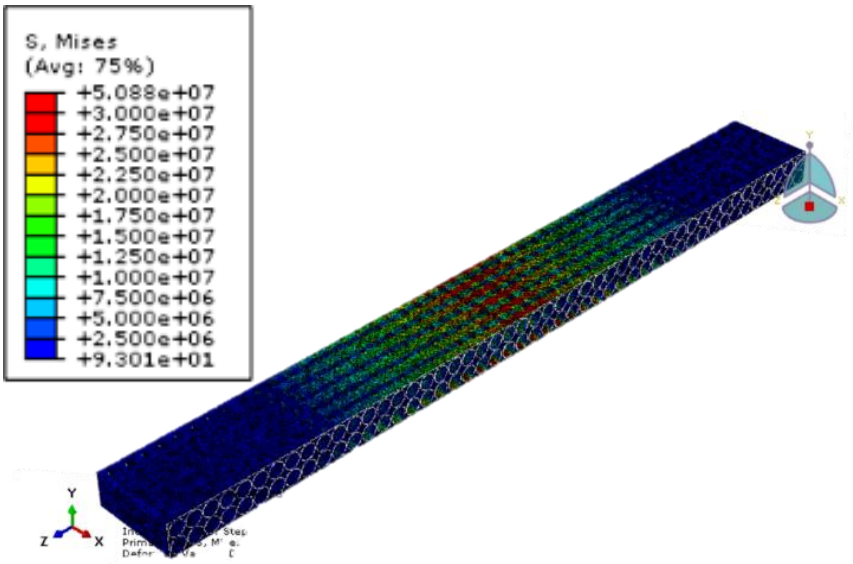

(a) 3D sample with longitudinal cross-section.

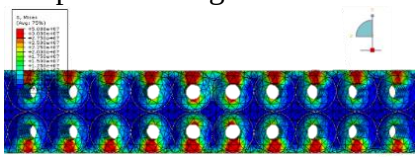

(b) longitudinal cross-section.

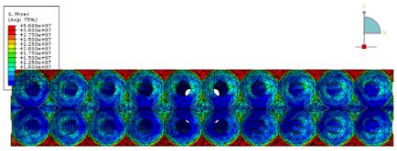

(c) longitudinal cross-section.

Fig. 7. Von-mises equivalent stress distribution of a 65 % volume fraction sample with uniform distribution of pores under bending loading.

Conversely, the location of the maximum value is difficult to be predicted in the bending samples with random pore size and distribution Fig. (8), because it depends on many factors, for example the distance from the neutral axis (more distance leads to more stress, therefore the highest stress located at the top or bottom of the uniform sample), the distance from the location of maximum bending moment (the centre of the sample in three points bending test), and the thickness of the walls the pores located near the upper and lower surfaces. therefore, the stress shows the non-uniform distribution and the maximum stress will be located at the weakest region with the thinnest horizontal walls at a region near the loading zone. On the other hand, the minimum stress located at the ends of the sample as shown in the side vertical section of the sample (see Fig. 8b).

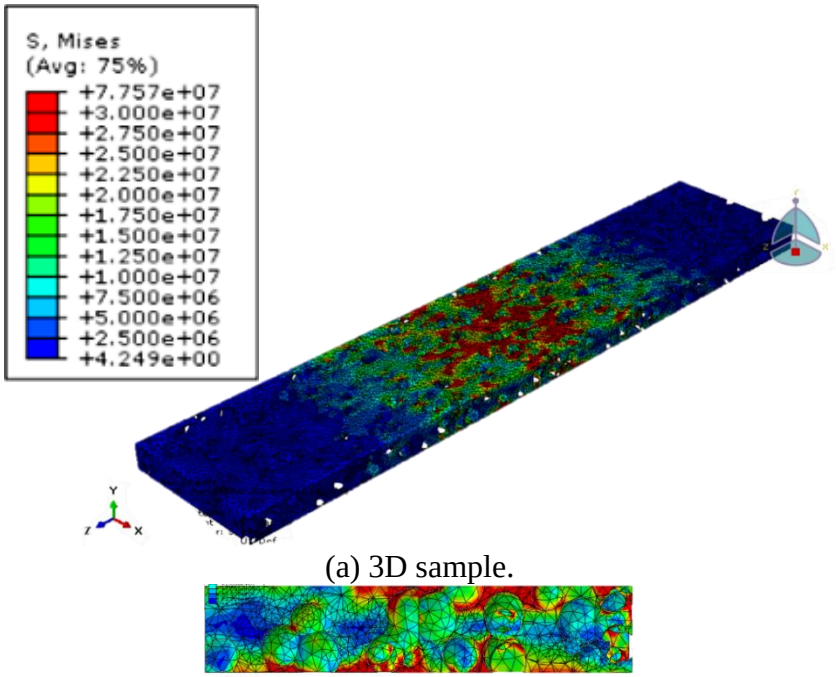

(a) 3D sample.

(b) longitudinal cross-section.

Fig. 8. Von-mises equivalent stress distribution of a 65 % volume fraction sample with a random distribution of pores under bending loading.

Fig. (9) shows the effect of porosity on the maximum Von-Mises stress for uniform and random distribution in bending specimens. In this case, the samples of uniform pores show a clear increase in maximum stress with increasing porosity from 15 to 40 %. Due to the increase in pore size which reduces the area carrying the load by reducing the thickness of the walls between the pores and the outer surface and as a result increases the stress. However, the maximum stress slightly decreases with increasing the porosity to 65 % due to the disappearing of the thin walls (the sample became open-cell porous material) at the upper and lower surfaces where the maximum stresses were developed in the lower porosity. Conversely, the samples with random porosity show a different behaviour, where the maximum stress slightly decreases with increasing porosity because sometimes samples with lower porosity may contain pores much closer to the outer surface (at the region of the maximum bending moment), which reduces the thickness of the walls and increases the stress.

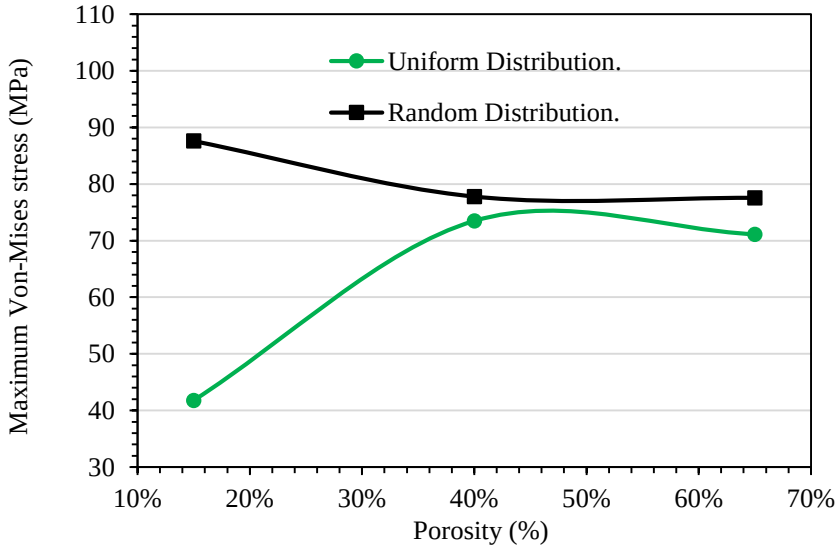

Fig. 9. The effect of pores volume fraction (porosity) on the Von-mises equivalent stress distribution of bending specimens for both uniform and randomly distributed pores.

3. CONCLUSIONS

An FE modeling investigation has been made to predict the mechanical behaviour of three-dimensional porous AA3003 samples, with uniform and random distribution of pores. Some concluding observations on the effects of the pore size, porosity and pores distribution on the mechanical behaviour are given below.

- The FE modelling was successful in predicting the location of the maximum stress for both the compression and bending test samples.
- The maximum Von-misses stress for the compression test of uniformly distributed pores is located in the vertical walls between pores. Whereas, the minimum values of stresses located at the horizontal walls between the pores. Moreover, the stresses showed almost uniform distribution all over the samples. Conversely, in the samples with random pore distribution, the maximum stress region was difficult to be predicted. However, the model shows that it is located at the thinnest vertical walls separated between random pores.
- In the bending test for a sample with uniform pore distribution, the maximum stress located at the area of maximum bending moment (loading line) either in the upper surface (the compression surface) or at the bottom surface (the tension surface) and the minimum value located at the ends of the sample. On the other hand, in the sample with random pore distribution, the model shows that the maximum stress is located in the thinnest horizontal walls near the upper or lower surface at the area of maximum bending moment.

Nomenclatures

a	constant
k	constant
P	property of foam
Ps	property of the cell wall material
Wt %	percent

Symbols

ρ	foam density
ρ_s	the density of the cell wall material

eviations

AA3003	Aluminium alloy 3003
FE modeling	Finite elements modeling

4. REFERENCES

[1] Liu, P.S.; and Chen, G.F. (2014). *Porous Materials: Processing and Applications* (1st ed.). Oxford, UK: Butterworth-Heinemann. Elsevier Ltd.

[2] Wheaton, R. (2016). Fundamentals of Applied Reservoir Engineering: Appraisal, Economics and Optimization (1st ed.). Gulf Professional Publishing. Elsevier Ltd.

[3] Gibson, L.J.; and Ashby, M.F. (1997). *Cellular Solids: Structure and Properties* (2nd ed.). Cambridge, UK: Cambridge University Press.

[4] Al-Zubaidy, B., Radhi, N. S., & Al-Khafaji, Z. S. (2019). Study the effect of thermal impact on the modelling of (titanium-titania) functionally graded materials by using finite element analysis. International Journal of Mechanical Engineering and Technology, 1.

[5] Falah, M. W., Ali, Y. A., Al-Mulali, M. Z., & Al-Khafaji, Z. S. (2020). Finite Element Analysis Of CFRP Effects On Hollow Reactive Powder Concrete Column Failure Under Different Loading Eccentricity. Solid State Technology, 63(2).
[6] Xu, Z. (2015). Fundamental Problems in Porous Materials: Experiments & Computer Simulation. Nebraska, USA: The University of Nebraska-Lincoln. Retrieved November 20, 2019, from https://digitalcommons.unl.edu/engmechdiss/41/
[7] Lefebvre, L.P.; Banhart, J.; and Dunand, D.C. (2008). Porous Metals and Metallic Foams: Current Status and Recent Developments. *Advanced Engineering Materials*, Special Issue: Metallic Foams, 10(9).
[8] Ashby, M.; Evans, T; Fleck, N.A.; Hutchinson, J.W.; Wadley, H.N.G.; Gibson, L.J. (2000). *Metal Foams: A Design Guide* (1st ed.). Burlington, MA, USA: Butterworth-Heinemann.
[9] Nammi, S. K.; Myler, P.; and Edwards, G. (2010). Finite element analysis of closed-cell aluminium foam under quasi-static loading. *Materials & Design*, 31.
[10] Kader, M.A.; Islam, M. A.; Hazell, P. J.; Escobedo, J. P.; Saadatfar, M.; and Brown, A. D. (2017). Numerical modelling of closed-cell aluminium foams under shock loading. *AIP Publishing. AIP Conference Proceedings 1793*, 120028.1-4
[11] Soro, N.; Brassart, L.; Chen, Y.; Veidt, M.; Attar, H.; Dargusch, M.S. (2018). Finite element analysis of porous commercially pure titanium for biomedical implant application. *Materials Science and Engineering: A*, 725.
[12] Tamai, T.; Muto, D.; Yoshida, T.; Sawada, M.; Suzuki, S.; Vesenjak, M.; Ren, Z. (2019). Compressive behavior of porous metals with aligned unidirectional pores compressed in the direction perpendicular to the pore direction. *Metallurgical and Materials Transactions A*,50(5).
[13] Nishi, M.; Tanaka, S.; Vesenjak, M.; Ren, Z.; Hokamoto, K. (2020). Experimental and computational analysis of the uni-directional porous (UniPore) copper mechanical response at high-velocity impact. *International Journal of Impact Engineering*, 136.
[14] Tomažinčič, D.; Vesenjak, M.; Klemenc, J.(2020). Prediction of static and low-cycle durability of porous cellular structures with positive and negative Poisson's ratios. *Theoretical and Applied Fracture Mechanics, 106.*
[15] Ling, Y.(1996). Uniaxial True Stress-Strain after Necking. *AMP Journal of* Technology,5.
[16] Chino, Y.; Mabuchi, M.; Yamada, Y.; Hagiwara, S.; Iwasaki, H. (2003). An Experimental Investigation of Effects of Specimen Size Parameters on Compressive and Tensile Properties in a Closed Cell Al Foam. *Materials Transactions*, 44(4).